Journal of Alloys and Compounds 849 (2020) 156319

Contents lists available at ScienceDirect

Journal of Alloys and Compounds

journal homepage: http://www.elsevier.com/locate/jalcom

Selective laser melting and tempering of H13 tool steel for rapid tooling applications

Michael Katancik [a, b], Saereh Mirzababaei [a, b], Milad Ghayoor [a, b], Somayeh Pasebani [a, b, *]

[a] School of Mechanical, Industrial and Manufacturing Engineering, Oregon State University, Corvallis, OR, 97330, USA
[b] Advanced Technology and Manufacturing Institute (ATAMI), Corvallis, OR, 97330, USA

ARTICLE INFO

Article history:
Received 16 November 2019
Received in revised form
22 June 2020
Accepted 6 July 2020
Available online 7 August 2020

Keywords:
Additive manufacturing
H13 tool steel
Selective laser melting
Tempering

ABSTRACT

H13 components with a relative density of ~99% were additively manufactured using the selective laser melting (SLM) process. The highest density part (relevant density 99%) with the lowest level of porosity (<0.01%) was made with a volumetric energy density of 760 J/mm^3 (152 W laser power, 100 mm/s scanning speed, 40 μm hatch spacing, and 50 μm layer thickness). Wrought and additively manufactured samples underwent tempering at 550, 600, and 650 °C for 2 h followed by furnace cooling. Additively manufactured samples and wrought H13 samples that were austenitized followed by water quenching were martensitic with similar microhardness values of 708.4 ± 25.0 HV and 708.1 ± 12.6 HV, respectively. A tempered martensitic structure was observed in SLM-manufactured and tempered samples. Samples that were additively manufactured and tempered at 550 °C showed higher microhardness (728.5 ± 28.2 HV) than non-tempered SLM-manufactured samples due to an upward shift in the secondary hardening phase. Tempering at 600 and 650 °C resulted in coarsening of the carbides and martensite, which led to a reduction in microhardness. Additively manufactured samples maintained higher microhardness values than wrought H13 samples at all tempering temperatures, likely because of higher dislocation density, finer grains present, and higher volume fraction of carbide nanoparticles.

© 2020 Elsevier B.V. All rights reserved.

1. Introduction

New design opportunities for additive manufacturing (AM) have presented themselves because of the increased demand for freedom in design and reduced material waste associated with current manufacturing methods. The field of tooling, in particular, plastic injection mold manufacturing and design, has the potential to benefit from rapid tooling (prototyping), design complexity, and capabilities to insert conformal cooling channels offered by AM [1,2]. Fabrication of metallic parts is possible via different types of AM techniques such as powder bed fusion, powder-feed methods, and wire-feed methods [3]. The type of AM explored in this study was selective laser melting (SLM), a process within the powder bed fusion methodology of AM. In SLM, component geometry is generated by melting powder layer by layer with a high-energy laser beam [4]. In this study, we examined H13 tool steel powder in the SLM process because of its excellent combination of ductility, hardness, and thermal fatigue resistance, making H13 an ideal candidate for molding and rapid tooling applications. Plastic injection molds are typically complex geometries that are challenging to manufacture with traditional, subtractive methodologies [1]. Additive processes provide significant key advantages over traditional subtractive machining processes through building up parts one layer at a time (typically between 10 and 50 μm in thickness), which allows for increasingly complex designs with small/internal features [5].

Four of the most influential processing parameters in SLM are laser power, laser scanning speed, hatch spacing, and layer thickness. One way to measure the amount of energy being delivered to the part is by using volumetric energy density (VED). VED is calculated using Equation (1) where P is laser power, v is laser scanning speed, σ is hatch spacing, and t is layer thickness [6].

$$VED = \frac{P}{v\sigma t}\left[\frac{J}{mm^3}\right]\# \quad (1)$$

If VED is too low, lack of fusion (LOF) between the powder particles occurs; if VED is too high, excessive evaporation occurs in

* Corresponding author. School of Mechanical, Industrial and Manufacturing Engineering (MIME), College of Engineering, Oregon State University, 2000 SW Monroe Ave, 204 Rogers Hall, Corvallis, OR, 97331, USA.
E-mail address: somayeh.pasebani@oregonstate.edu (S. Pasebani).

https://doi.org/10.1016/j.jallcom.2020.156319
0925-8388/© 2020 Elsevier B.V. All rights reserved.

the parts. LOF degrades mechanical properties of AM-manufactured parts and decreases relative density [7,8]. VED can be useful in determining processing parameters; however, Bertoli et al. [9] found that VED does not capture melt pool physics and therefore cannot be solely used to predict print quality.

ASTM H13 tool steel is a hot-worked tool steel with carbon content of 0.32–0.45 wt% [10]. H13 is commonly used for plastic injection molds because of its wear resistance while having good toughness and ductility to resist fatigue stresses common in mold usage [8,11]. Austenite, martensite, bainite, ferrite, and carbides are all possible microstructures depending on how H13 is heat treated, and more than one microstructure is typically found in a sample [12].

Previous studies on SLM of H13 have reported densities greater than 99% relative density [8,13–17] and evaluated VED values between 17.4 and 465.8 J/mm^3 with the highest relative densities found between VED of 60–120 J/mm^3 [8,18–20].

Mertens et al. [18] studied the impact of powder bed preheating on the microstructural and mechanical properties of SLM-manufactured H13 tool steel. They observed a fine cellular microstructure comprising of martensite and retained austenite phases that did not significantly change by different preheating temperatures. The mechanical properties of the SLM-manufactured parts and results of x-ray powder diffraction (XRD) showed that a preheating temperature of 400 °C resulted in formation of a different microstructure—the formation of bainite instead of martensite—suggesting that preheating could eliminate the necessity for post-processing tempering heat treatments [18].

Narvan et al. [8] investigated microstructure evolution of H13 fabricated via SLM. The microstructure of two samples manufactured at a VED of 62.5 J/mm^3, one with substrate preheating at 200 °C and one without preheating, contained martensite as the dominant phase along with retained austenite. Preheated samples showed 66% more retained austenite than samples without preheating possibly because of the slower quenching process experienced during preheating. They theorized the disappearance of the carbides was related to the rapid cooling during SLM, which highly restricts the diffusion mechanisms, hence impeding carbide precipitation. The highest relative density (99.7%) was obtained from a preheated sample at 200 °C. Additional microstructural characterization of all SLM samples showed fine equiaxed cellular-dendritic structure [9].

Krell et al. [19] studied the resulting microstructure of H13 manufactured via SLM using additional laser parameters and preheating temperatures (up to 300 °C). A relative density >99.5% was achieved for all samples. They reported that SLM-manufactured samples showed a fine-grained microstructure with a cellular arrangement consisting of about 75–80% ferrite and 20–25% γ-Fe that was not influenced by substrate preheating.

Preheating of the substrate reduces thermal stresses, which in turn lowers residual stresses and therefore reduces cracking [8,15]. A consequence of preheating the substrate is a greater concentration of retained austenite, which tends to reduce part quality; however, retained austenite can lead to enhanced fatigue life in certain applications [8,17,21–23]. Yan et al. [14] studied microstructures present in SLM H13 samples and found as-supplied H13 contained body-centered cubic (BCC)-structured α-Fe as the dominating phase, cementite (Fe_3C), and $(Cr,Fe)_7C_3$ phase. Microstructure of as-built SLM H13 consisted of martensite, retained austenite, and Fe_3C phase. Transmission electron microscopy (TEM) results revealed strong grain-growth orientation along the build direction.

Chen et al. [12] studied the effect of heat treatment on H13 samples produced by using direct energy deposition (DED) AM techniques at tempering temperatures of 350, 450, 550, 600 and 650 °C for 2 h followed by furnace cooling. They found that as-deposited samples contained martensite, fine carbides, and retained austenite. The authors [12] concluded that the presence of retained austenite was due to the rapid cooling rate associated with the DED processes. Rapid cooling suppresses carbide precipitation and growth, allowing more alloying elements to dissolve in the austenite, which reduces the martensite start transformation temperature.

In addition to microstructure, Chen et al. [12] measured mechanical properties of H13 manufactured via DED followed by heat treatment. Hardness values were measured to be 600 HV at a tempering temperature of 550 °C because of a high density of V-enriched needle-shaped carbides <15 nm. At temperatures above 550 °C hardness, values declined because of the emergence of lath martensite and coarsening of Cr-enriched particles slightly less than 100 nm. Another study found ductility to be poor in SLM-manufactured tool steel parts because of a heterogeneous microstructure and the residual stress concentrations. This poor ductility is a result of insufficient time for alloying elements to diffuse during rapid solidification of the melt pool [24].

Chen et al. [12] investigated the microstructure and mechanical properties of DED-manufactured and tempered H13, and Yan et al. [14] studied the microstructure of SLM-manufactured H13 without tempering. According to Krell et al. [19], after tempering SLM-manufactured H13 at elevated temperatures (>600 °C), the austenite phase disappeared; however, the cellular SLM structure remained unchanged, and no comparison was made with wrought H13.

The current knowledge on the microstructural evolutions and mechanical properties of SLM-manufactured and tempered H13 components is limited especially when compared with wrought H13. The ultimate goal of this study was to grow the knowledge base by evaluating the SLM followed by heat treatment as an alternative route to build H13 tool steel components that have similar or superior microstructure and mechanical properties than conventionally manufactured (wrought) H13 tool steel.

2. Experimental

2.1. Feedstock H13 tool steel powder

Spherical, gas-atomized ASTM H13 tool steel powder provided by Carpenter Technology Corporation was used in this work. The chemical composition of the powder is listed in Table 1 as provided by the manufacturer.

We identified the morphology and particle size by using an FEI QUANTA 600FEG scanning electron microscope (SEM). ImageJ, an image analysis software developed by the National Institute of Health (NIH), allowed for particle size analysis using the SEM micrographs. Using thresholding, we converted the greyscale micrographs into binary images that allowed the software to measure the particles present in the image. We conducted further particle size analysis by using the Malvern Mastersizer 3000E to measure particle size distribution using laser diffraction. For the wet method of dispersion, we used deionized (DI) water.

2.2. Powder characterization

We took apparent and tap density measurements on the H13 powder to characterize flow behavior and ensure sufficient flowability for the SLM process. Using a 25 cm^3 Hall flowmeter funnel, we found the apparent density by following test procedures set forth in ASTM B212. We collected tap density by using a 100 mL graduated cylinder and the Quantachrome Autotap machine. To collect tap density, we followed the test procedures established in

Table 1
Chemical composition of carpenter H13 powder (wt.%) [25].

Element	Fe	Cr	Mo	V	Mn	Ni	Si	C	P	S	Cu	N
Wt.%	90.05	5.16	1.43	1.03	0.42	0.20	1.06	0.42	0.02	0.01	0.07	0.03

Table 2
Elemental analysis of wrought H13 [26].

Element	C	Si	V	Cr	Mo	Mn	Fe
Wt.%	0.40	1.00	1.05	5.25	1.25	0.40	Bal.

ASTM B527.

2.3. Wrought H13 tool steel

We acquired wrought H13 tool steel from Cincinnati Tool Steel Company. The steel is manufactured via vacuum degassed tool steel ingots and hot worked for uniformity [26]. The chemical composition of the procured H13 tool steel is presented in Table 2 as provided by the manufacturer. Although the chemistry of the powder does not match that of the wrought steel samples, both lie within ASTM-accepted chemical ranges.

To ensure a completely homogeneous microstructure, we homogenized the wrought H13 samples. Samples were heated in the Rapid Temp Furnace by CM Inc. to 1050 °C with a heating rate of 10 °C/min and then homogenized for 2 h. At the conclusion of 2 h, we water quenched samples to obtain a fully martensitic microstructure.

2.3. SLM processing parameters

To achieve satisfactory material properties, we optimized the SLM processing parameters. The matrix of varying processing parameters we created resulted in 18 potential SLM processing parameters. While varying laser power and laser scanning speed, we kept the layer thickness and hatch spacing constant at 50 μm and 60 μm, respectively. The resulting matrix is presented in Table 3. We judged the quality of SLM-produced parts by using relevant density (collected using Archimedes density), and metallography to examine porosity and cracks. We chose a concentration of values between 60 and 120 J/mm^3 because of the high relative densities and part quality seen at these VED values in the literature [8,18–20].

2.4. SLM machine, conditions, and print specimen

To model the test specimen, manage SLM settings, and slice the specimen into layers, we used an ORLAS CREATOR SLM machine equipped with a spiral recoater and modelling software package. This machine has a 250 W ytterbium fiber laser, Ø100 × 100 mm build chamber, 20–100 μm powder layer thickness, and an argon or nitrogen inert atmosphere [27]. Using nitrogen to maintain an inert atmosphere, we kept oxygen levels inside the build chamber below 0.1 vol%. Preheating of the substrate was not possible with this SLM machine. The sample we used for testing was a cylindrical specimen measuring Ø8 x 11.5 mm. The test specimens can be seen during and after production in Fig. 1a and b, respectively. Support pillars and a support ring were modelled at the bottom of the specimen to provide support during the build process as well as aid in removal from the build platform at the conclusion of manufacturing.

Table 3
H13 printing parameters matrix; VED (J/mm^3) shown for corresponding laser speed and power.

		Laser Power (W)			
		152	177	203	228
Laser Speed (mm/s)	100	760.0	–	–	1140.0
	500	152.0	177.0	203.0	228.0
	800	95.0	110.6	126.9	142.5
	1100	69.1	80.5	92.3	103.6
	3000	25.3	29.5	33.8	38.0

2.5. Microstructure characterization and phase identification

To observe the grains, porosity, and microstructure, we prepared SLM-manufactured and wrought samples by using standard metallography technique. Using a Pace Technologies PICO155P precision cutting saw, we cross-sectioned samples and then encapsulated the samples in phenolic powder mounting compound by Pace Technologies using the TP-7001B mounting press by Pace Technologies. We then ground and polished the samples to a mirror-like finish using the NANO-2000T grinder-polisher by Pace Technologies. We examined the porosity by creating micrographs at 100X, 200X, 500X, and 1000X magnification using the Zeiss Axiotron microscope. ImageJ was used to threshold the images and identify porous and solid sections [15]. We performed phase identification in the mixed powder and fabricated samples by using XRD (Bruker AXS D8 Discover) with Cu Kα target, operated at 40 kV and 40 mA. For the XRD characterization, we used the step size of 0.05° and step time of 1 s. To examine microstructure, we etched the samples by submersion in a 2 vol% Nital solution (2 vol% nitric acid and 98 vol% ethanol). Etching time varied by sample and was done until the microstructure was exposed. We collected micrographs from etched samples in the same manner as the porous samples. On all wrought and SLM samples, we conducted additional microstructural characterization by using FEI Quanta 600 SEM coupled with electron dispersive X-ray spectroscopy (EDS).

2.6. Mechanical testing

To measure the microhardness values of the polished wrought and SLM-manufactured samples, we used the LECO LM 248AT microhardness tester. We recorded the Vickers hardness values using a 10 s dwell time and 300 g force. Ten random indentations were made for each specimen and the average microhardness value was reported.

2.7. Tempering heat treatment

To perform heat treatment, we used the same box furnace as we used for homogenization of the wrought H13 samples. We separated both the SLM-manufactured and wrought samples into four distinct groups that included control and tempering temperatures of 550, 600, and 650 °C. A ramp rate of 10 °C/min was used to reach the target temperature where the samples dwelled for 2 h followed by furnace cooling. We used the previously described metallographic process to collect optical micrographs and microhardness data on the heat-treated samples.

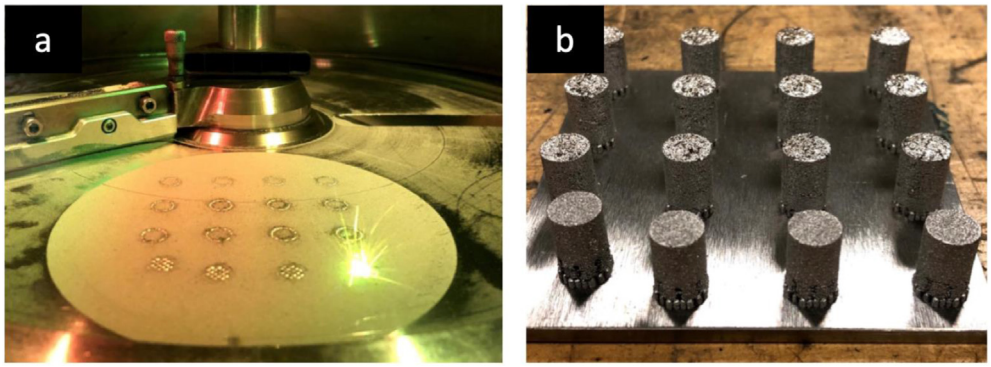

Fig. 1. (a) SLM process of H13 in an ORLAS CREATOR with a spiral recoater, and (b) matrix specimens of SLM processing parameters after printing, showing specimens and support structure.

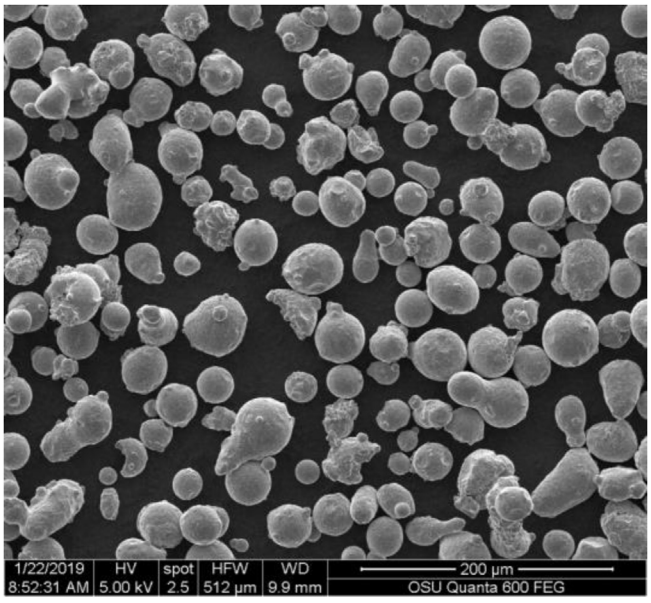

Fig. 2. SEM micrograph on H13 tool steel powder gas atomized by Carpenter Technology.

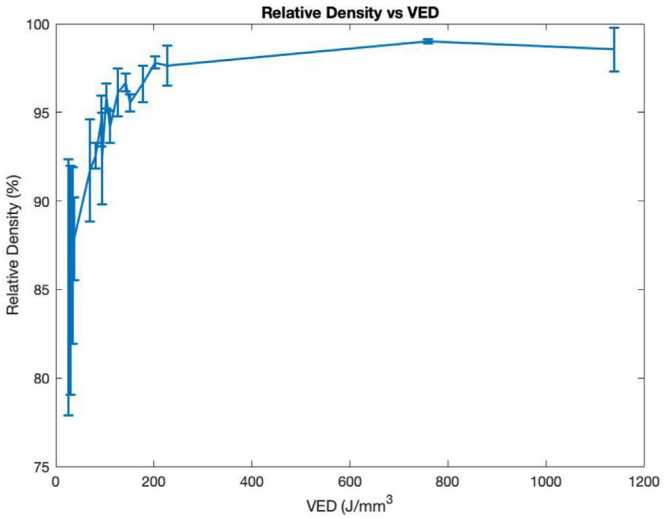

Fig. 3. Relative density of SLM-manufactured parts vs. VED.

3. Results

3.1. Powder analysis

The SEM micrographs of the gas-atomized process shown in Fig. 2 did not show consistent, spherical particles. Instead, many features such as satellites, craters, and elongated particles are present.

We used two separate methods to measure the particle size. Particle boundaries as discerned by Image J are presented in Fig. A.1 (page 22). We omitted boundary particles from analysis. An average particle size of 37.5 ± 25.0 µm was measured but likely has significant error due to the minimal sample size and inherent error in the thresholding method.

For a more accurate result, we used laser diffraction. We took 60 measurements with varying conditions to form the following results. Laser obscuration varied between 5.84 and 6.82% with an average value of 5.95%. The particle size distribution histogram of the 60 measurements is shown in Fig. A.2 (page 22). The median particle size (D_{50}) was found to be 36.2 µm; D_{10} and D_{90} were found to be 25.9 and 50.4 µm, respectively. We used D_{90} = 50.4 µm to determine that the layer thickness be set to 50 µm to allow ~90% of particles to fit within a single layer during manufacturing.

Apparent density for the powder had an average value of 3.94 ± 0.03 g/cm^3. The measured tap density of the powder was 4.76 g/cm^3. Therefore, tap density was 20.7% higher than apparent density measurements. The Hausner ratio, which is the ratio of tap to apparent density, was calculated to be 1.21. A low Hausner ratio such as in this case implies the powder has good flow character, meaning that it settles well during the powder spreading process associated with SLM.

3.2. Manufactured part density and optimization

We measured Archimedes density from the wrought, SLM printed, and heat-treated samples. A plot showing relative density vs. VED is presented in Fig. 3. Relative density was calculated against the average wrought sample density of 7.73 ± 0.05 g/cm^3.

The highest density was achieved at VED of 760 J/mm^3, which had a density of 7.65 ± 0.01 g/cm^3 and a relevant density of 99.0%. This sample did not have the highest VED, but the higher VED sample most likely had a significant amount of vaporization that led to a reduced density. In general, samples with higher VED values trended upward in density. We chose the sample with a VED of 760 J/mm^3 as the optimal processing parameters for creating multiple prints with the highest density for heat treatment. The

optimal processing parameters were identified as following: laser power of 152 W, laser scanning speed of 100 mm/s, layer thickness of 50 μm, and hatch spacing of 40 μm. We acknowledge a large deviation from the VED values seen in literature [8,18–20]. We believe high porosity coupled with low relative densities in the parts manufactured within the VED range found in literature to be a result of LOF, which suggested a higher VED was required. This led to the significantly higher VED value we chose to move forward in the study to heat treatment. When heat treated, the densities of the SLM-manufactured samples were within a single standard deviation of the non-heat-treated samples, and therefore no evidence suggested heat treating had any effect on enhancing density.

3.3. Microstructure characterization

Fig. 4 shows the phases we identified in XRD patterns obtained from H13 powder, wrought H13, homogenized wrought H13, SLM-manufactured, wrought H13 tempered at 650 °C, and SLM H13 tempered at 650 °C. The low-volume fraction of carbides resulted in them being unidentifiable using the XRD pattern. The XRD pattern of H13 powder shows peaks from a BCC phase and retained austenite face-centered cubic (FCC). The retained austenite at room temperature forms when the austenite phase does not fully transform to martensite. This happens because in steels with more than 0.3 wt% carbon, the martensite finish temperature is below room temperature [28]. Therefore, the existence of retained austenite in SLM-manufactured H13 is because of the high amount of carbon (0.4 wt%) and rapid solidification parts experience [19]. Similar to that seen in the SLM-manufactured parts, the H13 powder itself has a fraction of retained austenite, as shown in Fig. 4, because of the rapid cooling involved in powder production.

The H13 wrought alloy mainly consisted of a BCC phase, representing ferrite and martensite/bainite. Furthermore, the homogenized wrought H13, SLM H13, wrought H13 tempered at 650 °C, and SLM H13 tempered at 650 °C showed major peaks from a BCC phase combined with small traces of retained austenite with FCC structure in the matrix. Because the retained austenite in SLM H13 is an unstable phase at room temperature, upon tempering at 650 °C, the retained austenite transforms to ferrite. Therefore, the tempered samples of H13 show a lesser amount of retained austenite in the XRD pattern shown in Fig. 4. Holzweissig et al. [23] suggested a mechanism that when the top layer is being melted during SLM, the layers below within reach of the melt pool are being austenitized and quenched again. This repeated annealing and quenching of lower layers could cause carbon to diffuse, which stabilizes austenite and results in retained austenite at room temperature. This explanation would provide a reason for the presence of retained austenite in the samples even after undergoing heat treatment.

We examined porosity by using optical micrographs from the as-polished, prepared samples. Optical micrographs showing the most porous (VED = 25.3 J/mm^3) and least porous (VED = 760.0 J/mm^3) samples are presented in Fig. 5, which have porosities of 43% and 0.5%, respectively. The discrepancy between highest relative density (99.0%) and lowest porosity (0.5%) is most likely due to increased porosity near part edges in the skin hatch because porosity was measured in the centers of the cross section in the bulk hatch. Additionally, with the method of measurement being optical micrographs, the sample size was small, and we might not have examined large areas of porosity.

We observed cracks in the building direction of SLM-manufactured samples at higher VED as shown in Fig. 5b. We believe these cracks are caused by high thermal stresses associated with the SLM process. Because of the high temperature of the laser beam, the layers on top of the solidified layers would expand, while the colder underlying solidified layers would restrict this expansion. This expansion induces compressive stresses that could rise above the yield strength of the material and cause plastic deformation. Upon further cooling, the compressive state is converted into residual stresses, resulting in the formation of cracks within the SLM-processed material, called hot cracking. Preheating of the substrate has been shown as an effective method for reducing these residual stresses and eliminating cracking [8,15].

We also examined wrought H13 samples and analysis showed low porosity of less than 0.01%. This low porosity can be attributed to the manufacturing method of wrought H13, which includes fully melting the metal and hot rolling into a slab, resulting in low residual stresses and little gas entrained in the metal.

Fig. 6 shows optical micrographs of an etched homogenized wrought sample and an SLM sample. Homogenized wrought samples etched with a 2 vol% Nital solution revealed martensite needles, retained austenite, and ferrite grain boundaries. The needle martensite in the SLM sample was revealed and can be seen in Fig. 6b. The grains were revealed to be parallel to the build direction. High microhardness values in the homogenized wrought sample (708.1 ± 12.6 HV) and SLM sample (708.4 ± 25.0 HV) can be

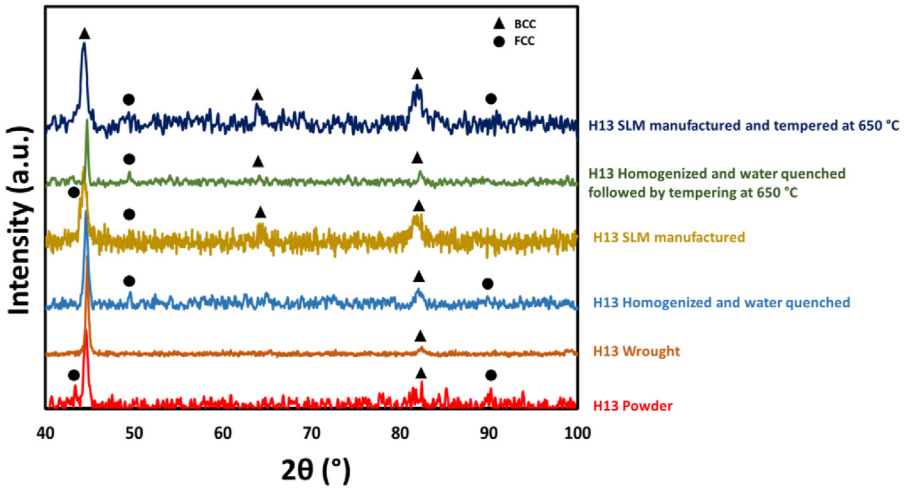

Fig. 4. XRD patterns obtained from H13 powder, wrought H13, homogenized wrought H13, SLM H13, wrought H13 tempered at 650 °C, and SLM H13 tempered at 650 °C.

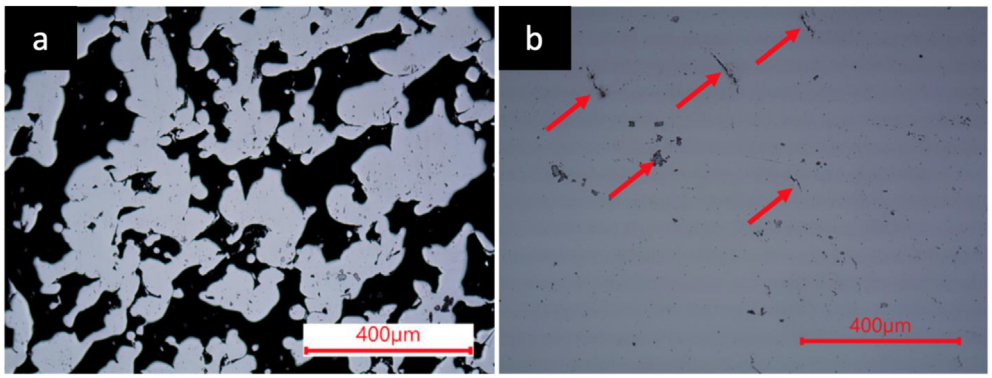

Fig. 5. Optical micrograph obtained from the as-polished surfaces of SLM-manufactured samples with (a) VED of 25.3 J/mm3 and (b) VED of 760.0 J/mm^3 (porosity and cracks are shown by arrows).

attributed to the fine martensitic microstructure presented in both micrographs. Melt pools were visibly acting as boundaries between groups of martensite as shown in Fig. 6b.

Fig. 7 shows the fine martensitic microstructure that comes from SLM manufacturing and fine dendritic-like retained austenite that can be explained by the extremely rapid heating and cooling present in the SLM process through a mechanism suggested by Holzweissig et al. [23].

Holzweissig et al. [23] observed a cell-like and elongated substructure arrangement of dislocations and retained austenite, and suggested the SLM process is similar to the quench and partitioning (Q + P) process in which the martensitic structure evolves as a result of rapid cooling. While melting a new layer, the solidified underneath layers are austenitized and quenched again. During this process, carbon is diffusing, which can stabilize austenite. Therefore, some of the austenite is stabilized and remains in the part at room temperature. Chen et al. [12] highlighted concerns associated with large quantities of retained austenite, which can negatively affect material wear resistance because this phase is thermodynamically unstable. Carbides might have been formed in the SLM samples, but we could not detect the carbides with SEM.

To eliminate the retained austenite in the samples, we tempered the samples at 550, 600 and 650 °C. Micrographs of etched and tempered samples are presented in Fig. 8. Significant changes were visible between the three different tempering temperatures. Fig. 8a–b shows homogenized wrought and SLM samples after tempering at 550 °C. The melt pool boundaries in the tempered SLM sample were less visible than the SLM sample presented in Fig. 6b.

Fig. 8c and d shows the SEM micrograph of homogenized wrought H13 and SLM-manufactured H13 after tempering at 600 °C. These samples also revealed a fine lath-type martensitic microstructure. We observed tempered martensite, ferrite (brighter contrast), and carbides (darker contrast and Fe_3C or cementite precipitates) for both wrought and SLM-manufactured samples. At 650 °C, a significant density of ferrite grains was present

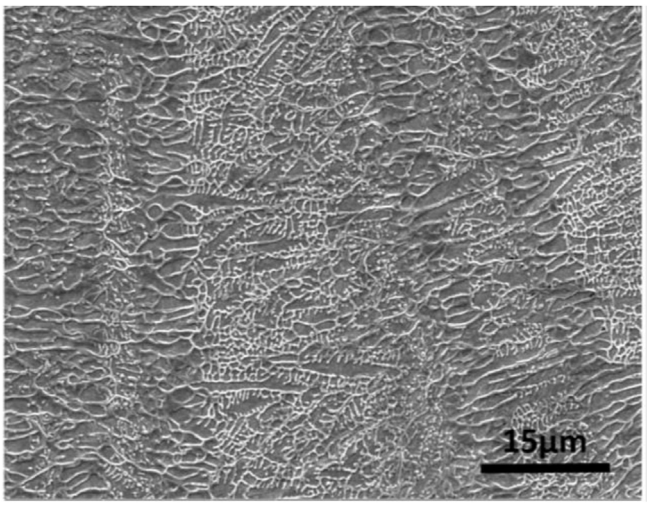

Fig. 7. SEM micrograph obtained from the parallel-to-building direction for an SLM-manufactured sample (VED = 760.0 J/mm^3), showing martensitic structure in SLM-manufactured samples.

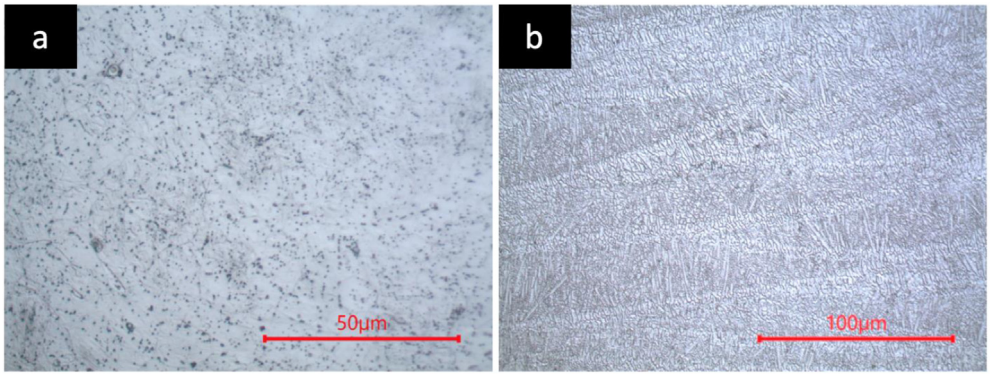

Fig. 6. Optical micrographs of (a) homogenized H13-wrought and (b) SLM-manufactured (VED = 760.0 J/mm^3) samples etched with 2 vol% Nital solution.

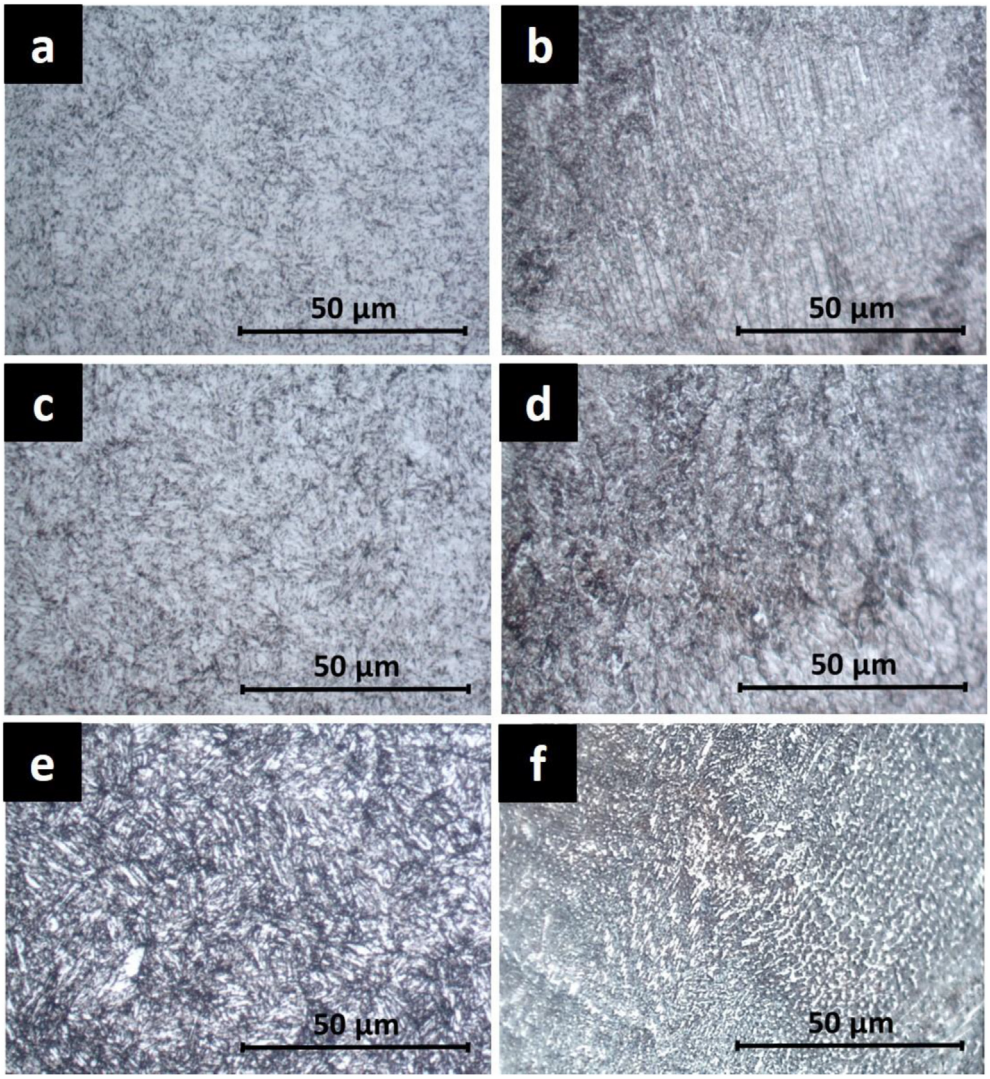

Fig. 8. Optical micrographs of tempered H13 tool steel etched with 2 vol% Nital solution: (a) wrought and tempered at 550 °C, (b) SLM manufactured and tempered at 550 °C, (c) wrought and tempered at 600 °C, (d) SLM manufactured and tempered at 600 °C, (e) wrought and tempered at 650 °C, (f) SLM manufactured and tempered at 650 °C.

throughout the microstructure, and lath martensite was less visible. This is shown for both the wrought and SLM-manufactured samples in Fig. 8e and f.

The SEM micrographs from the homogenized wrought and SLM-manufactured H13 after tempering at 550, 600 and 650 °C are presented in Fig. 9a–f, respectively. Fig. 9a and b shows the microstructure of wrought and SLM manufactured after tempering at 550 °C. We observed fine lath martensite in both wrought and SLM-manufactured samples. Fine carbides were hard to observe with SEM; however, we observed large carbide particles within the grains of the sample surface. After performing EDS on the samples, we found the wrought and SLM samples after tempering at 550 °C contained mostly vanadium carbides and molybdenum carbides, respectively. The SLM-manufactured and tempered (at 550 °C) sample had a microhardness value of 728.5 ± 28.2 HV, which was approximately 65 HV higher than the wrought H13 sample (661.7 ± 14.5 HV) tempered at the same temperature. The higher microhardness observed after SLM and tempering at 550 °C is likely because of a fine martensitic structure [16] super saturated with carbon and a high dislocation density that were reduced after tempering [12]. Neither sample in Fig. 9a and b showed signs of coarse precipitates along the grain boundaries. After DED and tempering H13 at 550 °C, a high volume fraction of fine V-enriched needle-shaped carbides in the range of 5–15 nm diameter were precipitated out from the α' matrix according to Chen et al. [12]. These coherent precipitates had a high thermal stability impeding the dislocation motion and enhancing the hardness through the dispersion mechanism [12].

After tempering at 600 °C, the microstructure was still lath martensite with a slight growth of the lath as shown in Fig. 9c and d for both the wrought and SLM-manufactured sample, respectively. A larger number of small carbide particles appeared within grains and along grain boundaries. EDS analysis revealed formation of chromium carbides and vanadium carbides for the SLM-manufactured sample. The microhardness values decreased in both wrought (616.1 ± 27.5 HV) and SLM-manufactured (686.8 ± 61.0 HV) samples because of the slight growth of lath-type martensite and slight growth of carbide particles.

At 650 °C, we observed precipitate coarsening along grain boundaries, and a significant density of ferrite grains was present throughout the microstructure. EDS analysis on both wrought and SLM-manufactured samples revealed the presence of carbides containing Fe, Cr, Mo, and V. Fig. 10 presents an SEM micrograph with EDS elemental analysis for an SLM sample tempered at 650 °C.

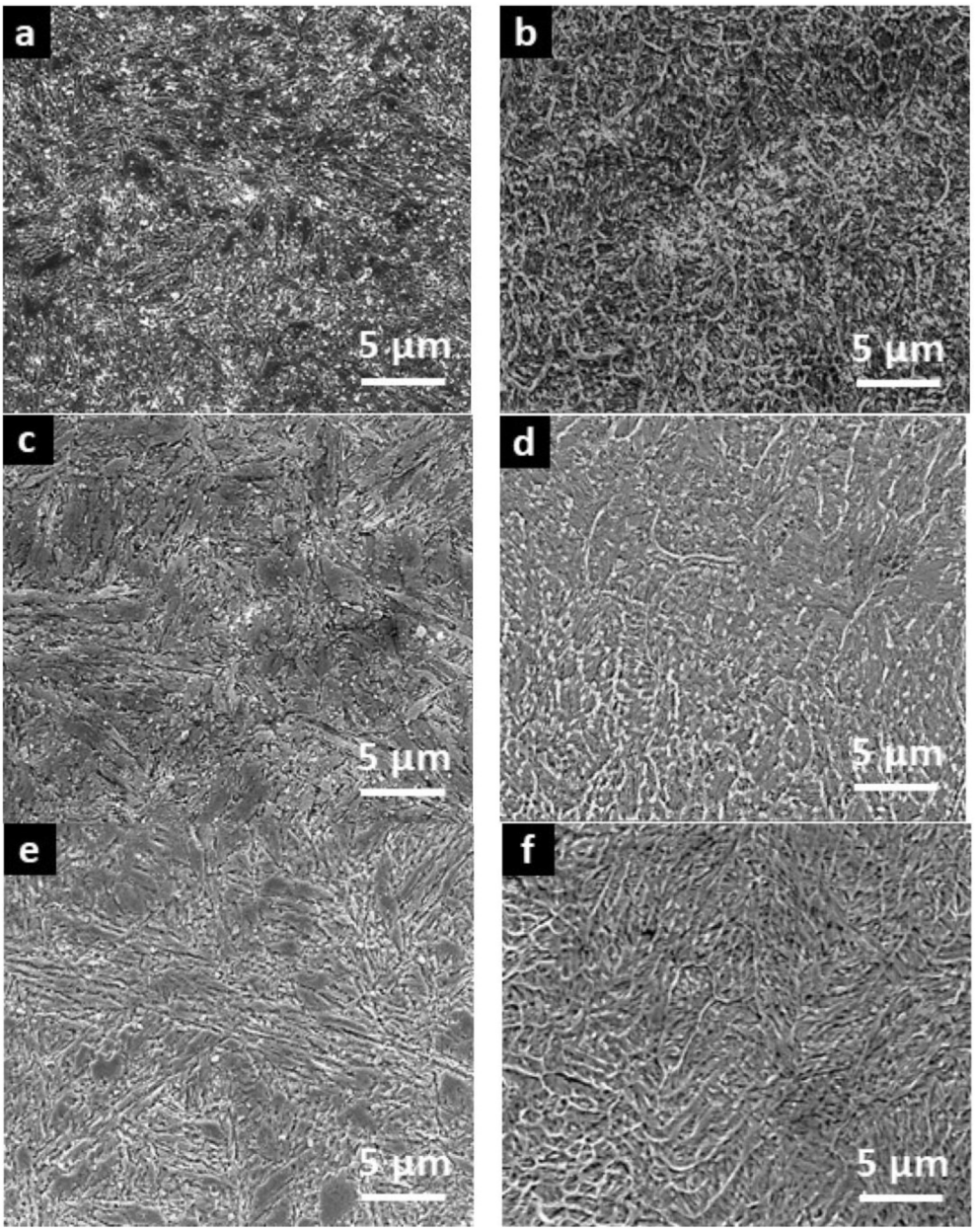

Fig. 9. SEM micrographs of tempered H13 tool steel etched with 2 vol% Nital solution: (a) homogenized wrought H13 tempered at 550 °C, (b) SLM tempered at 550 °C, (c) homogenized wrought H13 tempered at 600 °C, (d) SLM tempered at 600 °C, (e) homogenized wrought H13 at 650 °C, (f) SLM tempered at 650 °C.

We performed the EDS analysis, as shown in Fig. 10b, on the whole region of the SEM micrograph (revealing composition of matrix), spot 1 (S1), and spot 2 (S2). The compositional analysis of S1 (8.71 wt% C) and S2 (65.69 wt% C) indicated increased content of carbon compared to the matrix (0.94 wt% C), revealing the presence of carbides. Moreover, S1 analysis showed that the content of Mo, V, and Cr significantly increased compared to the matrix indicating appearance of carbides containing Mo, V, and Cr. However, elemental EDS analysis at S2 revealed the presence of carbides enriched in Fe and Cr. This is shown for both the wrought and SLM-manufactured samples in Fig. 9e and f, which revealed the grain boundaries, ferrite grains, and carbides. During tempering at 650 °C, carbon atoms diffused from martensite to form carbides. This was accompanied by the formation of ferrites, merging of lath martensite, and growth of carbides, which led to a reduction in microhardness values for both wrought (495.6 ± 8.2 HV) and SLM-manufactured (637.9 ± 52.5 HV) samples. Reduction in microhardness can lead to a higher ductility, further increasing the wear resistance of the material. According to Chen et al. [12] at a tempering temperature of 650 °C, carbon precipitates from the matrix-forming carbides of Mo_2C, VC, Cr_7C_3, and $M_{23}C_6$ where M can be Fe, Cr, or V with a diameters up to 100 nm.

3.4. Mechanical properties

We collected microhardness data on numerous samples with differing VED values during the processing parameters optimization portion of the study. These microhardness values with their corresponding VED values are presented in Fig. 11. We identified no meaningful trends between VED and microhardness data. We attributed this lack of trends to the uncorrelated relationship between VED and cooling rate published by Bertoli et al. [9] when

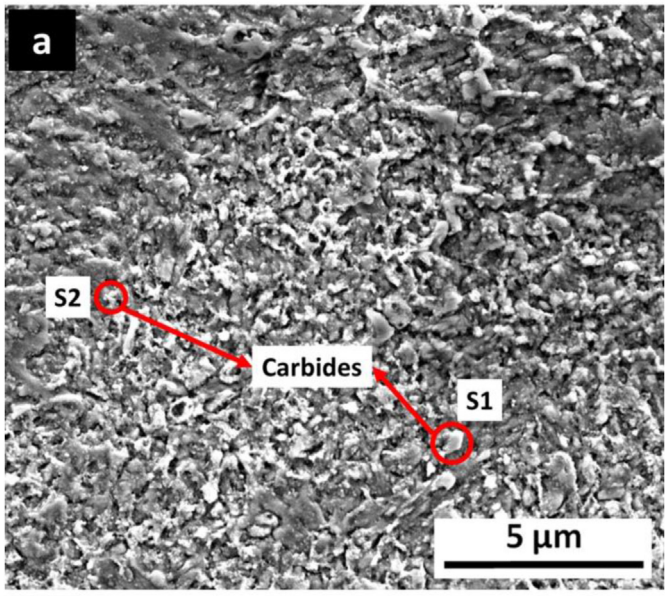

b

Matrix:		S1:		S2:	
Element	Wt %	Element	Wt %	Element	Wt %
C K	0.94	C K	8.71	C K	65.69
SiK	0.79	FeL	50.32	SiK	1.56
MoL	1.93	SiK	2.18	S K	0.00
V K	1.08	MoL	6.95	V K	0.00
CrK	5.09	V K	6.15	CrK	3.69
MnK	0.49	CrK	22.29	MnK	0.00
FeK	89.69	MnK	3.39	FeK	29.06
Total	100.00	Total	100.00	MoK	0.00
				Total	100.00

Fig. 10. a) SEM micrograph of tempered SLM H13 tool steel at 650 °C with b) corresponding EDS elemental compositions of matrix and carbides obtained from the two spots pointed out as circles.

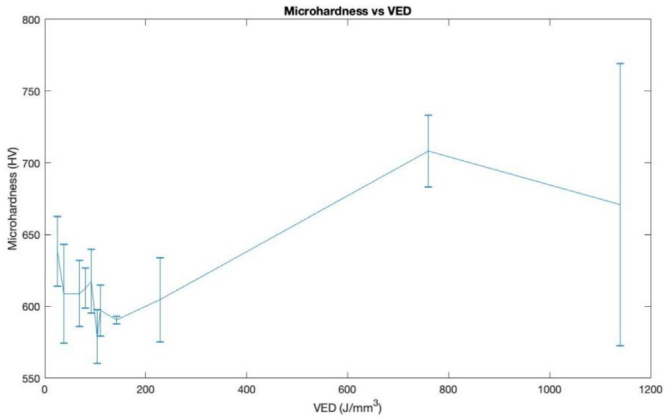

Fig. 11. Plot of microhardness versus VED of SLM-produced samples.

examining varied, single-track parameters with equal VED values. This study showed high laser powers with fast scanning speeds led to irregular morphology compared to low laser powers and slow scanning speeds.

We took microhardness measurements of the wrought H13 tool steel in its as-received form (201.9 ± 2.2 HV) and after undergoing homogenization followed by water quenching (708.1 ± 12.6 HV). The low microhardness value of the as-received wrought H13 can

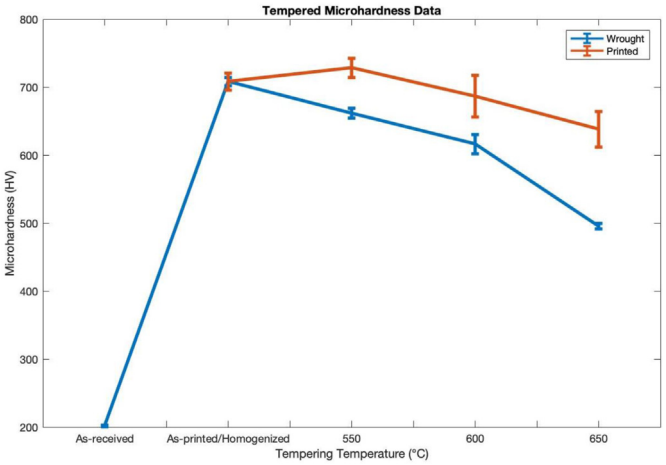

Fig. 12. Microhardness data for wrought and SLM-manufactured samples are shown as received wrought H13, as SLM-manufactured/homogenized wrought, tempered at 550, 600, and 650 °C.

likely be attributed to a softening heat treatment performed by the manufacturer on the stock to prepare the material for machining. In contrast, the homogenized wrought sample had a high microhardness because of its rapid water-quenched cooling and resulting fine martensitic microstructure. The microhardness of the SLM H13 is in agreement with the microhardness values of 650–689 HV found in Ref. [8].

Microhardness values for tempered wrought and SLM-manufactured samples are presented in Fig. 12. Both SLM-manufactured samples and homogenized and water-quenched wrought H13 samples were martensitic with similar microhardness values of 708.4 ± 25.0 and 708.1 ± 12.6, respectively. High hardness values suggest the large presence of a Fe-phase with BCC structure is a martensitic microstructure. Knowledge of the formation process also supports this presence because the wrought sample was homogenized and water quenched, and the SLM samples experienced rapid heating and cooling during manufacturing. However, with tempering, microhardness values decreased as tempering temperature increased. A notable deviation is the peak in hardness at 550 °C (secondary hardness peak) for the SLM-produced sample before beginning to decline at 600 °C. Tool steels show a secondary peak in hardness after precipitation of tempering carbide nanoparticles inside the matrix and along the grain boundaries [29]. As observed in Fig. 9b, many carbide nanoparticles precipitated from the matrix, which hinders the motion of dislocations. Therefore the peak in hardness at 550 °C could be explained by the formation of fine lath martensite as observed in Fig. 9b and formation of fine V-enriched carbides (5–15 nm) as reported by Chen et al. [12]. An additional factor that we believe increased hardness at 550 °C is the reduction in the amount of retained austenite in the samples.

By increasing the temperature from 550 °C to 650 °C, the hardness dropped from 728.5 ± 28.2 HV to 637.9 ± 52.5 HV in the SLM-manufactured sample. This drop in the hardness could be attributed to the combined effect of accelerated carbide coarsening at higher temperatures, softening of the martensitic matrix because of a reduction in dislocation density and recovery, and merging of the lath-type martensite [12]. Wrought samples displayed significantly lower hardness with lower standard deviations than the SLM-manufactured samples at all three tempering temperatures. For example, at 650 °C, the SLM-manufactured sample had a significantly higher microhardness value of (637.9 ± 52.5 HV) than the wrought sample (495.6 ± 8.2 HV). The higher standard

deviation of SLM samples might be attributed to the presence of micro defects and microstructural inhomogeneity [19]. Generally, higher hardness in SLM-processed samples shows evolution of a predominant martensitic microstructure in the steel during SLM [23]. Furthermore, the higher hardness in SLM-manufactured samples at different tempering temperatures compared to wrought samples can be explained after description of high thermal stability of retained austenite in the SLM sample.

Austenite in the SLM-processed samples is supersaturated in alloying elements and accordingly has a noticeably lower martensite start temperature. Stabilization of retained austenite in SLM samples is due to segregation of interstitial solute atoms to austenite dislocations and to interfaces of austenite and martensite. However, the retained austenite in SLM samples differs from that in wrought samples. The main fraction of retained austenite in wrought samples decomposes at lower tempering temperatures, whereas austenite in SLM samples transforms at higher tempering temperatures (about 600 °C) [30]. Therefore, secondary hardening of SLM samples occurs by transformation of austenite to martensite as well as precipitation of carbides within the refined microstructure while in the wrought samples, the major means of hardening is dispersion hardening of BBC phase by alloy carbides.

Lower diffusion of alloying elements in austenite compared to martensite leads to a delay in precipitation of tempering carbides in the austenite phase of SLM samples and shifts secondary max hardness to an elevated temperature (compared to conventional manufactured), making SLM H13 tool steel a potential candidate for high-temperature applications [19].

In summary, the combined effect of the following factors caused higher hardness in SLM samples at all tempering temperatures compared to wrought samples: (1) shifted secondary hardening to higher temperature because of delayed precipitation of tempering carbides in high thermally stable retained austenite, (2) higher residual stresses formed by the high solidification rate in SLM, (3) formation of a cellular substructure in the SLM process that does not disappear after tempering at 700 °C according to Krell et al. [19], and (4) grain refinement because of laser rapid solidification [19,23,31].

4. Conclusions

H13 tool steel components with a density of ~99% were additively manufactured using the SLM process. The highest density part (relative density 99%) with the lowest level of porosity was made with a VED of 760 J/mm^3 (152 W laser power, 100 mm/s scanning speed, 40 μm hatch spacing, and 50 μm layer thickness). Density, microhardness, phases, and microstructure of SLM-manufactured H13 were compared with those of wrought H13 tool steel parts. Furthermore, the effect of tempering at 550, 600, and 650 °C (10 °C/min during heating, then homogenized for 2 h followed by furnace cooling) was also examined in SLM-manufactured H13 tool steel and wrought H13 tool steel samples. The primary findings of this study are as follows:

1. Optical microscopy of polished SLM samples showed higher VED values correlated with decreased remained porosity. The least porous SLM-manufactured sample (VED of 760.0 J/mm^3) was measured to be 0.5% porous by area fraction. However, SLM-manufactured parts showed signs of cracking in the build direction, leading to concerns of potential fatigue fracture in operation and plastic injection molding. The optimal VED found in this study was significantly higher than VED values in the literature because of observation of LOF in manufactured parts at lower energies.
2. Homogenized wrought H13 samples and SLM-manufactured H13 tool steel samples showed similar microhardness values of ~708 HV. Wrought samples exhibited a microstructure mainly composed of martensite, second-phase precipitates, and retained austenite. SLM samples consisted of a fine martensite and fine dendritic-like retained austenite that could be explained by the repeated homogenizing and quenching as layers are built up. Meta-stable retained austenite can be explained in both samples by the quenching temperature being greater than the martensite finish temperature.
3. The H13 wrought alloy mainly consisted of ferrite and martensite. The homogenized wrought, SLM-manufactured, wrought tempered at 650 °C, and SLM tempered at 650 °C samples showed major peaks from ferrite and martensite combined with small traces of retained austenite in the matrix. Although still exhibiting peaks, tempered samples of H13 showed a lesser amount of retained austenite. A repeated austenitizing of subsequent layers during SLM could cause carbon to diffuse and stabilize the austenite, which results in retained austenite at room temperature.
4. SLM-manufactured and tempered samples had the highest microhardness value of 728.5 ± 28.2 HV at 550 °C, which was part of a secondary hardness peak because of the precipitation of tempering carbides that were too small to be detected by SEM. Fine martensitic structure and high dislocation density caused during rapid solidification of SLM and presence of carbides formed during tempering could potentially hinder dislocation movement and lead to higher hardness values. At 600 and 650 °C, precipitates formed during tempering showed slight coarsening, and more carbon was diffused from the martensite to form carbides, leaving a low carbon and ductile ferritic matrix behind. SLM samples likely have higher microhardness values than wrought samples because of a shifted secondary hardening temperature, higher residual stresses from manufacturing, a cellular substructure formed during SLM, and grain refinement from laser rapid solidification.

CRediT authorship contribution statement

Michael Katancik: The first author, Michael Katancik is an Honors College senior under graduate student in Mechanical Engineering who conducted most of the selective laser melting experiments and characterized the microstructure and mechanical properties of the H13 tool steel samples. **Saereh Mirzababaei:** The second author, Saereh Mirzababaei is a PhD student in Mechanical Engineering who prepared the samples for microstructural analysis and obtained the SEM micrographs. **Milad Ghayoor:** The third author, Milad Ghayoor is a PhD student in Materials Science who trained Michael in SLM process and helped with XRD experiment, data analysis and retained austenite written part. **Somayeh Pasebani:** Dr. Somayeh Pasebani is an assistant professor at Oregon State University who leads this research and is corresponding author.

Declaration of competing interest

The authors declare that they have no known competing financial interests or personal relationships that could have appeared to influence the work reported in this paper.

Acknowledgements

The first author acknowledges financial support provided by the Honors College at Oregon State University. This project was

supported by a grant received from the Oregon Manufacturing Innovation Center (OMIC). We acknowledge the support of the Advanced Technology and Manufacturing Institute (ATAMI) director and staff as well as Teresa Sawyer at the Oregon State Electron Microscopy Center.

Appendix

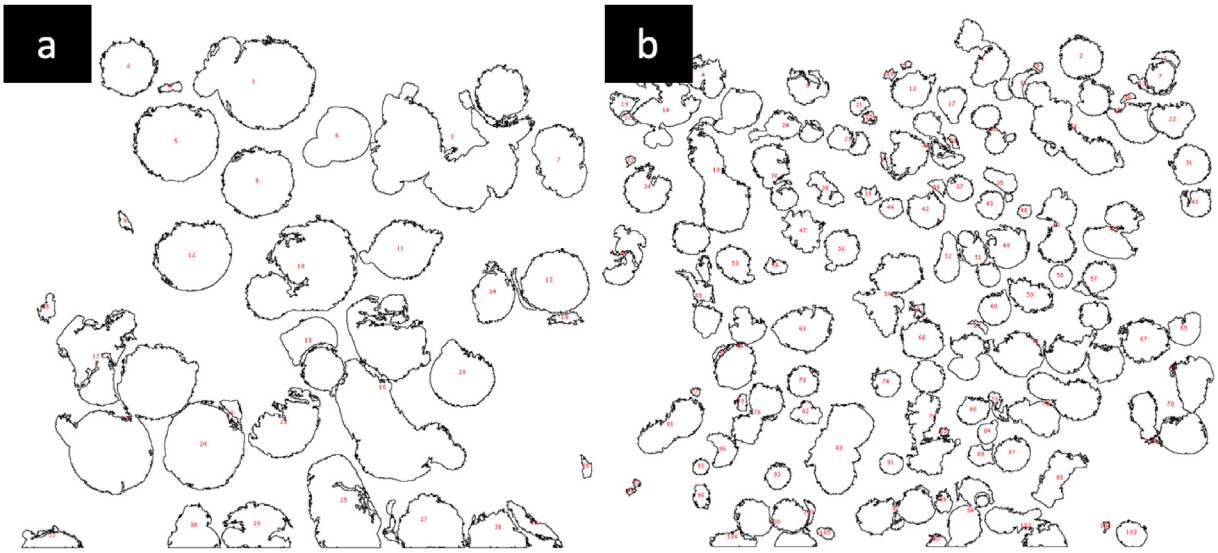

Fig. A.1. Discerned particle outlines using Image J of (a) a highly magnified micrograph and (b) a lower magnified micrograph.

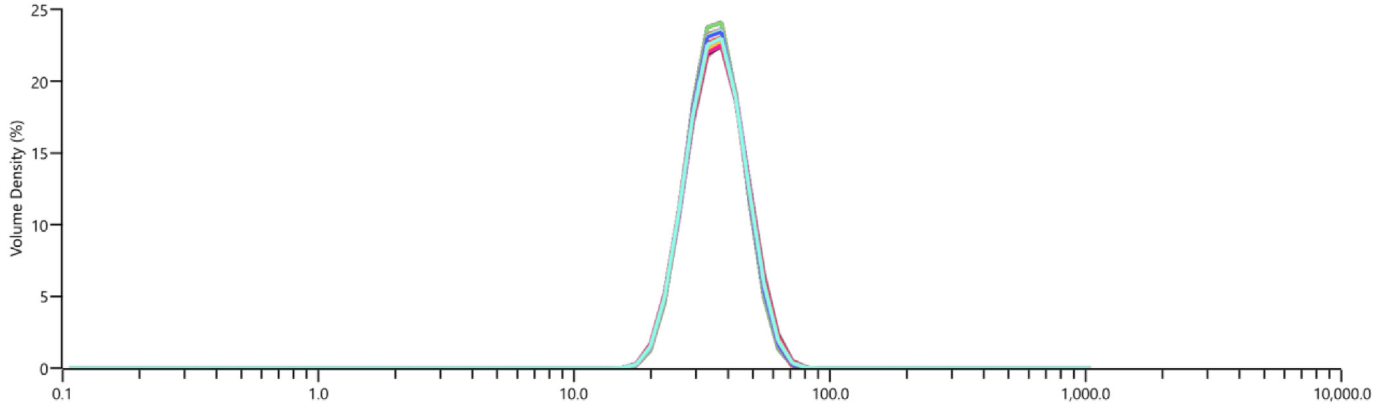

Fig. A.2. Particle size distribution histogram for all measurements of the H13 powder. X-axis is powder size in μm on a logarithmic scale.

References

[1] M. Simonelli, C. Tuck, N.T. Aboulkhair, I. Maskery, I. Ashcroft, R.D. Wildman, R. Hague, A study on the laser spatter and the oxidation reactions during selective laser melting of 316L stainless steel, Al-Si10-Mg, and Ti-6Al-4V, Metall. Mater. Trans. 46 (2015) 3842–3851, https://doi.org/10.1007/s11661-015-2882-8.

[2] E. Sachs, E. Wylonis, S. Allen, M. Cima, H. Guo, Production of injection molding tooling with conformal cooling channels using the three dimensional printing process, Polym. Eng. Sci. 40 (2000) 1232–1247, https://doi.org/10.1002/pen.11251.

[3] S. Mirzababaei, S. Pasebani, A review on binder jet additive manufacturing of 316L stainless steel, J. Manuf. Mater. Process. 3 (2019) 82, https://doi.org/10.3390/jmmp3030082.

[4] M. Ghayoor, S. Mirzababaei, K. Lee, Y. He, C. Chang, B.K. Paul, S. Pasebani, Strengthening of 304L stainless steel by addition of yttrium oxide and grain refinement during selective laser melting, in: Proc. 30th Annu. Int. Solid Free. Fabr. Symp., Austin, TX, 2019.

[5] W.J. Sames, F.A. List, S. Pannala, R.R. Dehoff, S.S. Babu, The metallurgy and processing science of metal additive manufacturing, Int. Mater. Rev. 61 (2016) 315–360, https://doi.org/10.1080/09506608.2015.1116649.

[6] G. Telasang, J. Dutta Majumdar, G. Padmanabham, M. Tak, I. Manna, Effect of laser parameters on microstructure and hardness of laser clad and tempered

AISI H13 tool steel, Surf. Coating. Technol. 258 (2014) 1108–1118, https://doi.org/10.1016/j.surfcoat.2014.07.023.
[7] H.D. Carlton, A. Haboub, G.F. Gallegos, D.Y. Parkinson, A.A. MacDowell, Damage evolution and failure mechanisms in additively manufactured stainless steel, Mater. Sci. Eng. 651 (2016) 406–414, https://doi.org/10.1016/j.msea.2015.10.073.
[8] M. Narvan, K.S. Al-Rubaie, M. Elbestawi, Process-structure-property relationships of AISI H13 tool steel processed with selective laser melting, Materials 12 (2019) 2284, https://doi.org/10.3390/ma12142284.
[9] U. Scipioni Bertoli, A.J. Wolfer, M.J. Matthews, J.-P.R. Delplanque, J.M. Schoenung, On the limitations of volumetric energy density as a design parameter for selective laser melting, Mater. Des. 113 (2017) 331–340, https://doi.org/10.1016/j.matdes.2016.10.037.
[10] A01 Committee, Specification for tool steels alloy, ASTM International, n.d. https://doi.org/10.1520/A0681-08R15.
[11] Tool Steels, 1972.
[12] C. Chen, K. Yan, L. Qin, M. Zhang, X. Wang, T. Zou, Z. Hu, Effect of heat treatment on microstructure and mechanical properties of laser additively manufactured AISI H13 tool steel, J. Mater. Eng. Perform. 26 (2017) 5577–5589, https://doi.org/10.1007/s11665-017-2992-0.
[13] M. Mazur, P. Brincat, M. Leary, M. Brandt, Numerical and experimental evaluation of a conformally cooled H13 steel injection mould manufactured with selective laser melting, Int. J. Adv. Manuf. Technol. 93 (2017) 881–900, https://doi.org/10.1007/s00170-017-0426-7.
[14] J.J. Yan, D.L. Zheng, H.X. Li, X. Jia, J.F. Sun, Y.L. Li, M. Qian, M. Yan, Selective laser melting of H13: microstructure and residual stress, J. Mater. Sci. 52 (2017) 12476–12485, https://doi.org/10.1007/s10853-017-1380-3.
[15] P. Laakso, T. Riipinen, A. Laukkanen, T. Andersson, A. Jokinen, A. Revuelta, K. Ruusuvuori, Optimization and simulation of SLM process for high density H13 tool steel parts, Phys. Procedia. 83 (2016) 26–35, https://doi.org/10.1016/j.phpro.2016.08.004.
[16] B. Ren, D. Lu, R. Zhou, Z. Li, J. Guan, Preparation and mechanical properties of selective laser melted H13 steel, J. Mater. Res. 34 (2019) 1415–1425, https://doi.org/10.1557/jmr.2019.10.
[17] H. Chen, D. Gu, Effect of metallurgical defect and phase transition on geometric accuracy and wear resistance of iron-based parts fabricated by selective laser melting, J. Mater. Res. 31 (2016) 1477–1490, https://doi.org/10.1557/jmr.2016.132.
[18] R. Mertens, B. Vrancken, N. Holmstock, Y. Kinds, J.-P. Kruth, J. Van Humbeeck, Influence of powder bed preheating on microstructure and mechanical properties of H13 tool steel SLM parts, Phys. Procedia. 83 (2016) 882–890, https://doi.org/10.1016/j.phpro.2016.08.092.
[19] J. Krell, A. Röttger, K. Geenen, W. Theisen, General investigations on processing tool steel X40CrMoV5-1 with selective laser melting, J. Mater. Process. Technol. 255 (2018) 679–688, https://doi.org/10.1016/j.jmatprotec.2018.01.012.
[20] M. Mazur, M. Leary, M. McMillan, J. Elambasseril, M. Brandt, SLM additive manufacture of H13 tool steel with conformal cooling and structural lattices, Rapid Prototyp. J. 22 (2016) 504–518, https://doi.org/10.1108/RPJ-06-2014-0075.
[21] H. Chen, D. Gu, D. Dai, M. Xia, C. Ma, A novel approach to direct preparation of complete lath martensite microstructure in tool steel by selective laser melting, Mater. Lett. 227 (2018) 128–131, https://doi.org/10.1016/j.matlet.2018.05.042.
[22] W. Cui, D. San-Martín, P.E.J. Rivera-Díaz-del-Castillo, Stability of retained austenite in martensitic high carbon steels. Part I: thermal stability, Mater. Sci. Eng. 711 (2018) 683–695, https://doi.org/10.1016/j.msea.2017.10.102.
[23] M.J. Holzweissig, A. Taube, F. Brenne, M. Schaper, T. Niendorf, Microstructural characterization and mechanical performance of hot work tool steel processed by selective laser melting, Metall. Mater. Trans. B 46 (2015) 545–549, https://doi.org/10.1007/s11663-014-0267-9.
[24] H. Chen, D. Gu, D. Dai, C. Ma, M. Xia, Microstructure and composition homogeneity, tensile property, and underlying thermal physical mechanism of selective laser melting tool steel parts, Mater. Sci. Eng. 682 (2017) 279–289, https://doi.org/10.1016/j.msea.2016.11.047.
[25] D. Carpenter, Product Certification, 2018.
[26] Cincinnati Tool Steel Company, AISI H13, 2018. http://cintool.com/documents/mold_quality/H13.pdf. (Accessed 1 September 2018).
[27] The Machine—Orlas Creator, Coherent Laser, 2019. http://creator.or-laser.com/en/the-machine/. (Accessed 26 August 2018).
[28] G. Thomas, Retained austenite and tempered martensite embrittlement, Metall. Trans. A. 9 (1978) 439–450, https://doi.org/10.1007/BF02646396.
[29] H. Berns, W. Theisen, G. Scheiblein, Ferrous Materials: Steel and Cast Iron, Springer, Berlin, 2008.
[30] R. Colaço, R. Vilar, Effect of laser surface melting on the tempering behaviour of din X42Cr13 stainless tool steel, Scripta Mater. 38 (1997) 107–113, https://doi.org/10.1016/S1359-6462(97)00441-7.
[31] M. Wang, W. Li, Y. Wu, S. Li, C. Cai, S. Wen, Q. Wei, Y. Shi, F. Ye, Z. Chen, High-temperature properties and microstructural stability of the AISI H13 hot-work tool steel processed by selective laser melting, Metall. Mater. Trans. B 50 (2019) 531–542, https://doi.org/10.1007/s11663-018-1442-1.